

# Full-Length Envelope Analyzer (FLEA): A tool for longitudinal analysis of viral amplicons

Kemal Eren<sup>1</sup>, Steven Weaver<sup>2</sup>, Robert Ketteringham<sup>3</sup>, Morné Valentyn<sup>3</sup>, Melissa Laird Smith<sup>4,5</sup>, Venkatesh Kumar<sup>6</sup>, Sanjay Mohan<sup>6</sup>, Sergei L Kosakovsky Pond<sup>2</sup>, Ben Murrell<sup>6\*</sup>

**1** Bioinformatics and Systems Biology, University of California San Diego, La Jolla, CA, USA

**2** Department of Biology, Temple University, Philadelphia, PA, USA

**3** University of Cape Town, Cape Town, Western Cape, South Africa

**4** Icahn School of Medicine at Mount Sinai, One Gustave L Levy Place, Box 1498, New York, NY 10029

**5** Icahn Institute of Genomics and Multiscale Biology, One Gustave L Levy Place, Box 1498 New York, NY 10029

**6** Division of Infectious Disease, Department of Medicine, University of California San Diego, La Jolla, CA, USA

\* [bmurrell@ucsd.edu](mailto:bmurrell@ucsd.edu)

## ABSTRACT

Next generation sequencing of viral populations has advanced our understanding of viral population dynamics, the development of drug resistance, and escape from host immune responses. Many applications require complete gene sequences, which can be impossible to reconstruct from short reads. HIV-1 *env*, the protein of interest for HIV vaccine studies, is exceptionally challenging for long-read sequencing and analysis due to its length, high substitution rate, and extensive indel variation. While long-read sequencing is attractive in this setting, the analysis of such data is not well handled by existing methods. To address this, we introduce FLEA (Full-Length Envelope Analyzer), which performs end-to-end analysis and visualization of long-read sequencing data.

FLEA consists of both a pipeline (optionally run on a high-performance cluster), and a client-side web application that provides interactive results. The pipeline transforms FASTQ reads into high-quality consensus sequences (HQCSs) and uses them to build a codon-aware multiple sequence alignment. The resulting alignment is then used to infer phylogenies, selection pressure, and evolutionary dynamics. The web application provides publication-quality plots and interactive visualizations, including an annotated viral alignment browser, time series plots of evolutionary dynamics, visualizations of gene-wide selective pressures (such as  $dN/dS$ ) across time and across protein structure, and a phylogenetic tree browser.

We demonstrate how FLEA may be used to process Pacific Biosciences HIV-1 *env* data and describe recent examples of its use. Simulations show how FLEA dramatically reduces the error rate of this sequencing platform, providing an accurate portrait of complex and variable HIV-1 *env* populations.

A public instance of FLEA is hosted at <http://flea.datamoney.org>. The Python source code for the FLEA pipeline can be found at <https://github.com/veg/flea-pipeline>. The client-side application is available at <https://github.com/veg/flea-web-app>. A live demo of the P018 results can be found at <http://flea.murrell.group/view/P018>.

## INTRODUCTION

Next generation sequencing (NGS) has become an invaluable tool for studying HIV-1 and other rapidly evolving viruses by providing direct high resolution measurements of viral genetic diversity within the host. NGS has been used to study immune escape [1–7], drug resistance [7–13], transmission bottlenecks [10,14–16], population structure and dynamics [2,3,17–23], tropism dynamics [24], and multiplicity of infection [25]. It is also used in clinical virology [26,27]. For reviews of the promises and challenges of NGS applications in virology, see [28], [29], [30], and [31].

Full-length sequences can resolve features that are difficult to assemble from short sequences [8,32]. For instance, Pacific Biosciences SMRT sequences were able to resolve 1.5 kb *msg* isoforms from *Pneumocystis jirovecii*, but reads from a 454 instrument could not be assembled correctly [32]. For tracking evolutionary patterns in viral populations, accurately resolving these features provides a more accurate history of the population, which becomes especially relevant when epistatic interactions and linkage between mutations effect phenotypic changes in the pathogen [33–35]. For example, studies of HIV-1 *env* frequently use functional assays to measure the potency with which a given antibody or donor serum neutralizes a specific *env* strain [36], which requires knowing the full *env* sequence.

We have developed a pipeline for handling long read HIV-1 *env* sequencing data from within-host viral populations: the Full-Length Envelope Analyzer (FLEA). FLEA addresses the specific challenges posed by large volumes of such data, e.g., using the sequencing protocols we previously described in Laird *et al* [37], which also contains an overview of a prototype of FLEA. Here we describe the full pipeline and experimentally demonstrate its ability to resolve populations of closely related variants. FLEA uses state-of-the-art tools and methods at every step and can be accessed through a web browser or on a high-performance cluster. FLEA is readily extensible to other genes and systems.

FLEA has recently been used by the authors in two high-profile studies. In [38], we describe how FLEA was used to process PacBio HIV-1 *env* data from a clinical trial of monoclonal antibody 10-1074. For sequences sampled before and after therapy, FLEA reveals that prior to antibody therapy low-frequency *env* variants were present with mutations that typically confer resistance to 10-1074. Additionally, when resistance emerges, it emerges multiple times, exploiting many different resistance pathways. FLEA was also used to characterize the longitudinal *env* population that drove development of a broadly neutralizing antibodies against the apex of the *env* trimer, sampled from donor PC64 from the Protocol C primary infection cohort [39].

There exist dozens of standalone pipelines developed for analyzing HIV-1 and related sequence data, including longitudinal samples [4,9,13,40]. However, it was necessary to develop a new tool due to HIV-1 *env*'s extensive natural indel variation and the high rate of indels in long PacBio reads, which are especially problematic when any spurious indel in the 2.6kb *env* amplicon corrupts the reading frame, rendering the sequence uninterpretable. With HIV-1 *env*, the common strategy of mapping reads to a reference fails because the diversity in variable regions of *env*, predominantly driven by extensive indel processes, means that these regions in sampled reads lack homology to those in any heterologous reference sequence. Instead, FLEA relies on a fine-grained cluster-and-consensus strategy to remove spurious indels from reads. The task is related to Liang *et al.* (2016), but, rather than distinguishing a small number of variants at 81-91% identity, we must distinguish potentially hundreds of variants that differ by only a handful of bases.

In addition to a standalone application, FLEA is also available as an online resource that provides interactive visualizations for all its analyses. To allow researchers to further examine and dissect their results, FLEA also provides access to raw data, such as aligned consensus sequences and phylogenetic trees.

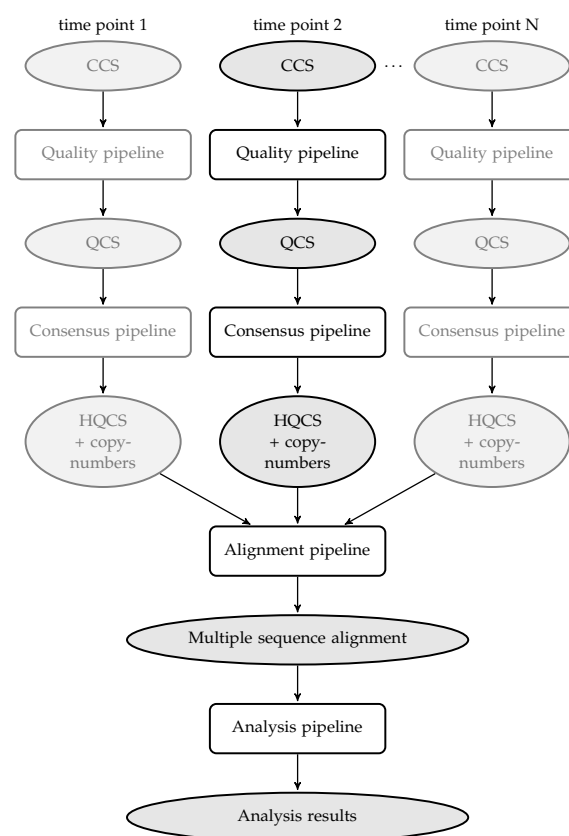


**Figure 1.** Overview of the entire pipeline, broken into conceptual sub-pipelines. The Quality and Consensus sub-pipelines process each time point separately. Duplicate steps in other time points are grayed out. CCS stands for “circular consensus sequences”; QCS for “quality-controlled sequences”, and HQCS for “high-quality consensus sequences”.

## DESIGN AND IMPLEMENTATION

### Pipeline

The input to FLEA is a set of FASTQ files from the PacBio RS-II or Sequel. Each set corresponds to one time point, containing circular consensus sequence (CCS) reads, which can be obtained using the “Reads of Insert” protocol on PacBio’s SMRTportal or SMRTanalysis tools. Upon completion, the FLEA pipeline produces results as JSON (Javascript Object Notation) files, a standard format for machine (and human-) readable structured data. The logic of FLEA is implemented in Nextflow [41], a workflow framework for deploying parallel pipelines to clusters and clouds.

FLEA consists of multiple sub-pipelines, as shown in Fig. 1. Details of the quality and consensus pipelines are depicted in Fig. 2. Together, these two pipelines take error-prone CCS reads and convert them into unique high-quality consensus sequences. The alignment pipeline generates a multiple sequence alignment, which is used by multiple methods in the analysis pipeline.

### Quality assurance sub-pipeline

The first steps remove low quality reads and filter out common sequencing artifacts. Parameters given in these steps were chosen for full-length HIV-1 envelope sequences from the RS-II or Sequel

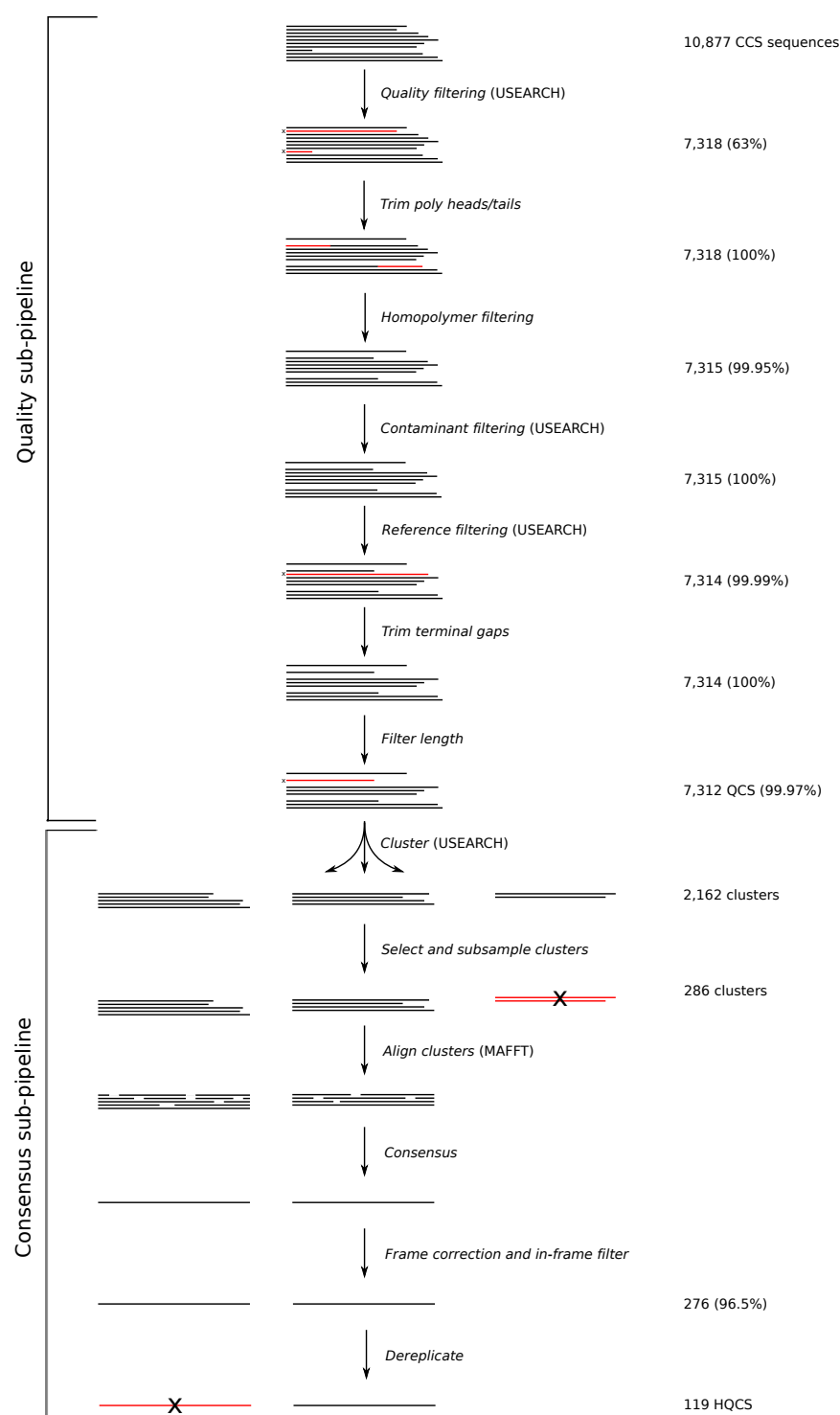


**Figure 2.** Combined view of the quality and consensus sub-pipelines. These steps are repeated independently on each time point. Numbers are reported from the analysis of sequences from the first time point (V03) of donor P018, which is 3 months post infection. Percentages give the fraction of sequences retained after filtering. Tasks indicate whether they use third-party tools *USEARCH* or *MAFFT*.

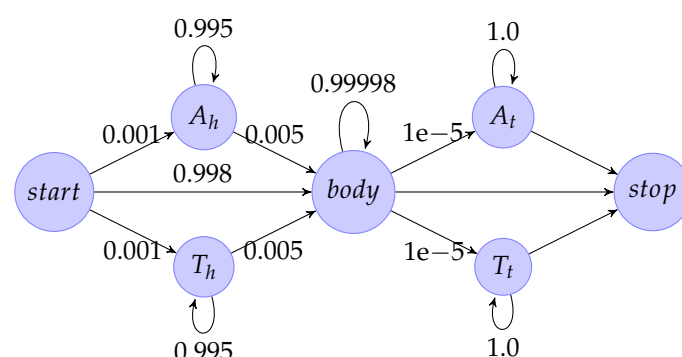


**Figure 3.** Hidden Markov model used for trimming poly-A and poly-T heads and tails. A head and tail states have a small ( $p = 0.01$ ) probability to emit non-A bases, and similarly for T. The body state emits all four bases with equal probability. The start, and stop states emit nothing.

platforms. Other reads with different properties (error rates, error models, lengths, homopolymer distributions, etc.) likely require different parameters. All steps are run independently per time point.

1. **Filter by error rate.** The input FASTQ files contain Phred scores for each base, encoding the probabilities of incorrect base calls. USEARCH [42] is used to remove reads with an expected error rate greater than 1%, computed as the mean of the per-base error probabilities.
2. **Trim heads/tails.** A fraction of reads from the Laird *et al.* sequencing protocol contain poly-A or poly-T heads or tails (cause unknown), which can be hundreds of bases long and sometimes contain a small number of other bases.

These heads and tails are trimmed with a hidden Markov model (Fig. 3) implemented in Pomegranate [43]. The emission probabilities of the model were fixed, and the transitions trained using Baum-Welch. The Viterbi path for each sequence is computed, and bases emitted by head and tail nodes are removed.

3. **Filter long runs.** Reads with homonucleotide runs longer than 16 bases are discarded. This length was chosen to be twice the length of the longest such run in the LANL HIV database [44].
4. **Filter contaminants and trim reads.** Sample contamination can introduce non-native sequences that interfere with subsequent analyses, so these contaminants must identified and discarded. USEARCH is used to compare reads to a contaminant database and a reference database using `usearch_global`. Alignments returned from querying the database are then used to trim reads to the gene boundaries. Trimming terminal insertions is vital for the accuracy of downstream tasks, such as length filtering and clustering.

The contaminant database contains HXB2 and NL4-3 *env*, each ubiquitous in labs working with *env* sequences and a common source of sample contamination. Reads that match with  $\geq 98\%$  identity are discarded. Since a 1% error rate cutoff was earlier used, this parameter conservatively ensures that these contaminants are almost certainly identified.

The reference database contains thirty-eight sequences representing the major HIV-1 Group M subtypes from the LANL sequence database [44]. Reads with  $\leq 70\%$  identity to every sequence in the reference database are discarded. This cutoff is chosen to retain reads remotely similar to HIV-1 Group M while excluding contaminants such as human or

bacterial genome reads. If a sample is from SIV, or from a non group-M HIV+ donor, then more appropriate reference sequences should be added to the database.

5. **Filter by length.** By default, sequences shorter than 90% or longer than 110% of the length of the reference sequence are discarded. However, sequences with large deletions are frequently observed in HIV. These likely represent replication incompetent envelopes, and their reduced length can cause them to be dramatically oversampled due to PCR length bias. Users who want to include these species in their analyses should modify these parameters.

Reads that pass this quality assurance phase have low expected error rates and no homonucleotide runs, are within 70% identity of at least one reference sequence, are (after trimming) no more than 10% different in length than a reference sequence, and do not match the contaminant database. We refer to these sequences as quality-controlled sequences (QCS).

### Consensus sub-pipeline for variant identification

Even for highly diverse populations, unique reads in a sequencing run outnumber the true unique variants, predominantly due to sequencing errors. The problem is far more significant in long reads than in short reads, precluding the use of amplicon denoising strategies used to reduce error rates in short read sequencing [45]. To accommodate this effect, the next phase of the FLEA pipeline clusters and combines QCS reads, attempting to infer the true variants in each time point. It also attempts to detect and correct frameshift errors.

1. **Cluster.** USEARCH is used with the `cluster_fast` command to generate clusters with 99% nucleotide identity. This parameter approximates the 1% error cutoff used in the error rate filtering step, so that pairwise distances of sequences in the same cluster are consistent with the sequencing error. `cluster_fast` runs in a single pass, so it is sensitive to input order. Sequences are sorted from lowest to highest quality according to expected error rate; experiment suggests that this order yields better results (see supporting information).
2. **Select and subsample clusters.** Clusters with fewer than three members are discarded, because they are too small to de-noise by majority consensus. Clusters with more than 50 members are subsampled to the top 50 with the lowest expected error rate to speed up the multiple sequence alignment step.
3. **Align and consensus.** MAFFT [46] is used to align each cluster. The consensus sequence of each alignment is computed.
4. **Frame correction** In-frame consensus sequences from all time points are collected into a USEARCH database for frame correction. `usearch_global` is then used to align each out-of-frame sequence to its top hit. The nucleotide alignment is used to correct incomplete codons: short insertions (1 or 2 base pairs) are discarded, and single deletions are replaced with the aligned base. Sequences with longer insertions or deletions are discarded. All changes are logged, so that the user can identify the sequences that have been corrected.
5. **Uniqueness** Non-unique consensus sequences are dereplicated using `usearch -fastx_uniques`.
6. **Copy numbers** The number of sequences per cluster provides an estimate of the relative abundance of that HQCS in the population. Those numbers are further augmented by adding sequences orphaned by cluster filtering and HQCS dereplication. `usearch_global` is used to assign each QCS to its nearest HQCS. The number of sequences accrued by each HQCS is interpreted as its copy number.

All of these tasks are run separately for each time point, yielding sets of unique in-frame consensus sequences. We refer to these sequences as high-quality consensus sequences (HQCS).

### Alignment sub-pipeline

The HQCSs from all time points are combined into a single file, translated to protein sequences, and aligned using MAFFT. A Python script then transfers the gaps from each aligned protein sequence to the corresponding nucleotide sequences to produce a codon-level nucleotide multiple sequence alignment of all unique variants from all time points.

### Analysis sub-pipeline

The analyses used in FLEA take as input the two outputs of the alignment phase: a codon multiple sequence alignment of all unique HQCS sequences from all time points, and their associated copy numbers. These data are used for the following analyses.

1. **Time point metrics.** HyPhy [47] scripts are used to compute evolutionary metrics (total,  $dN$ , and  $dS$  divergence and diversity) and phenotypic metrics (protein length, potential N-linked glycosylation sites, isoelectric point) for each annotated region (e.g., V1, MPER) in the amplicon for each time point.
2. **MRCA.** The most recent common ancestor is inferred by taking the copy-number-weighted codon consensus of the codon-aligned HQCSs from the earliest time point. By including gaps, the MRCA sequence is already aligned with the rest of the multiple sequence alignment. This strategy is acceptable for primary infection studies from single founders with very low early diversity.
3. **Reference coordinates.** MAFFT is used to assign HXB2 [48] coordinates to the gapped MRCA sequence, which are then transferred to the full multiple sequence alignment.
4. **Infer phylogeny.** A maximum-likelihood phylogenetic tree is inferred with FastTree2 [49,50] under the general time reversible model.
5. **Ancestral sequence reconstruction.** HyPhy is used to infer ancestral sequences at the internal nodes of the phylogeny, using joint maximum likelihood reconstruction and the HKY85 substitution model [51].
6. **Multidimensional scaling.** TN93 [52] is used to compute a distance matrix for all HCQC sequences using the Tamura Nei 93 distance [53]. Metric multidimensional scaling [54] (implemented in `scikit-learn` [55]) is used to find a two-dimensional embedding of the sequences that approximates their pairwise distances.
7. **FUBAR.** Site-specific selection rates are inferred using FUBAR [56], implemented in HyPhy.
8. **Position-specific changes.** Entropy and Jensen-Shannon divergence are computed for each position in each time point.

The results of these analyses are provided to the user in an interactive web application, described next.



## Web application

The FLEA web app is built using modern web design principles. It consists of two parts: a Javascript client-side app, written using the Ember.js [57] framework, and a server-side REST (REpresentational State Transfer) service for serving JSON-formatted data. There are two main benefits to using this decoupled pattern for scientific web applications. First, the client-side code only needs to be downloaded once, at the start of the session. The data are requested from the server and cached as needed. Once everything is loaded, the visualizations run entirely in the browser with no delays for page loads. Second, the REST service may be reused by other apps and third-party tools.

The web app presents the results of the FLEA analysis as a series of interactive visualizations. The report is organized into the following sections.

**Multidimensional scaling.** A two dimensional embedding of the HQCSs is visualized as a bubble plot, showing changes in population structure over time, as shown in Fig. 4. This visualization has been especially useful for investigating populations with superinfection, or with multiple founders, where aggressive recombination between vastly different *env* variants precludes the use of phylogenies.

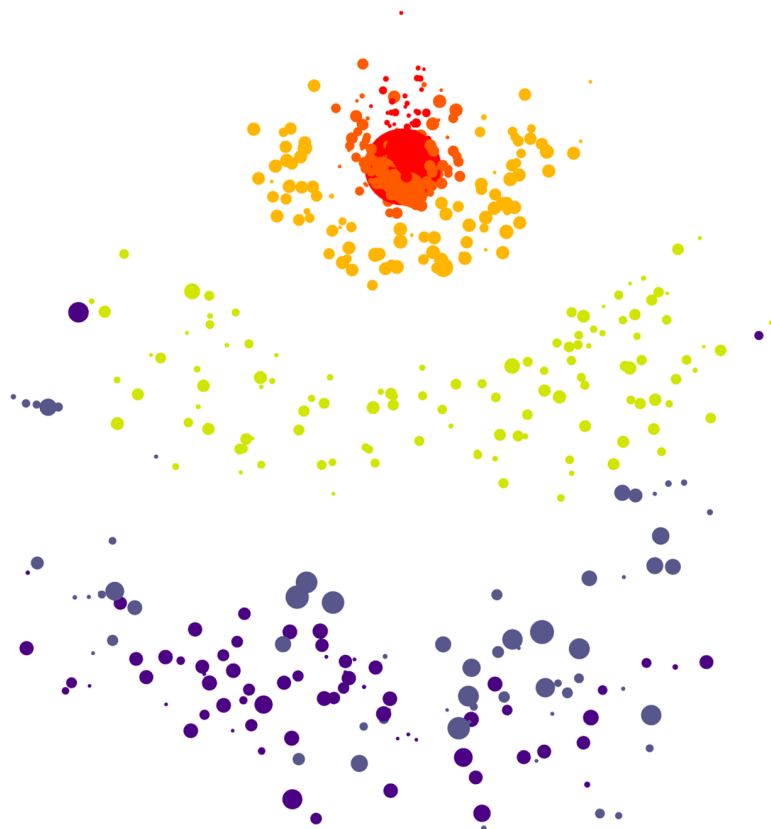


**Figure 4.** Screenshot of the multidimensional scaling plot. The embedding in two dimensions preserves pairwise evolutionary distances between HQCSs. Node area is proportional to copy number, and color corresponds to time point. The increasing genetic diversity of the population is visible as time goes on.



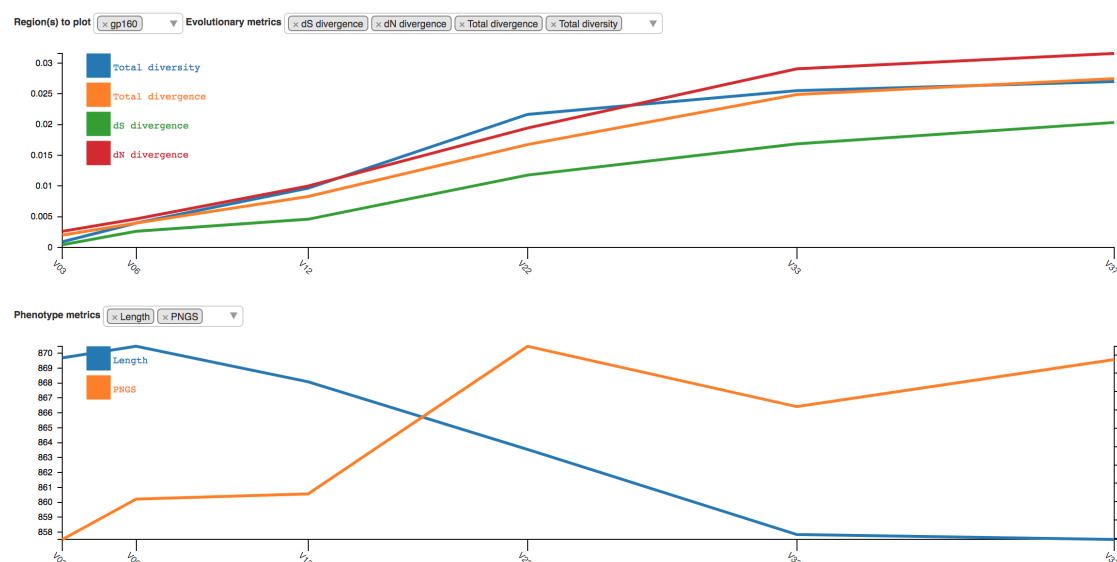


**Figure 5.** Screenshot of the evolutionary trajectory report. Four evolutionary metrics (*dS* divergence, *dN* divergence, total divergence, and total diversity) and two phenotype metrics (length and possible N-linked glycosylation sites) are shown for gp160.

**Evolutionary trajectory.** The evolutionary trajectory viewer plots evolutionary and phenotypic metrics for each time point and multiple regions in the amplicon, giving a high-level overview of population dynamics over time. Fig. 5 shows the plot for the entire gp160 region of HIV-1 Env, which is generated with the D3.js plotting library [58].

**Sequences.** The multiple sequence alignment of all the HQCSs sequences is the foundation for all subsequent analyses. It is displayed in the amino acid sequences viewer, which contains a custom alignment browser and an interactive motif dynamics plot, as shown in Fig. 6.

**Protein structure.** The protein structure viewer maps evolutionary metrics to an interactive three-dimensional structure of the protein, customized from PDB ID 5FUU, a recently resolved cryo-EM structure [59], and rendered using pv [60]. Missing residues are rendered as spheres which are positioned by Bézier curve interpolation. *dN/dS* ratios, Jensen Shannon divergence, and entropy may all be mapped to the protein structure, as shown in Fig. 7. The same metrics are also plotted in one dimension for each time point, as shown in Fig. 8. The protein visualization interacts with the sequence viewer by showing alignment positions and highlighting the residues in the selected sequence motif.

**Trees.** The tree viewer renders a tree browser with *phylotree.js* [61], as shown in Fig. 9. Leaf nodes are scaled to the copy number of their sequence. The tree zoom level, layout, and coloring is interactively modifiable. Motifs selected in the sequence viewer are mapped to the tree. Ancestral nodes are colored by motif, allowing inferred changes to be tracked through the entire phylogeny.

**Figure 6.** Screenshot of amino acid sequences viewer. Sequences are grouped by identity, with aggregate copy number and population percentage shown to the right. An overview of the amplicon, optionally annotated with region names, provides fast access to different locations of the alignment. Selecting columns of the alignment interactively updates the amino acid dynamics plot, showing the dynamics of the selected motif over time. In this case, the trajectory shows changes in the N332 glycan supersite. Sites inferred by FUBAR to be undergoing positive selection are selectable.

## RESULTS

The entire pipeline was run on HIV-1 *env* reads from donor P018, which are available from the NCBI Sequence Read Archive under BioProject PRJNA320111, and were sequenced as part of [37] on the RS-II instrument, using the older generation P5/C3 PacBio sequencing chemistry. The full dataset contains 58,468 CCS reads. The reads are split across six time points, which are coded as V03, V06, V12, V22, V33, and V37, where  $Vx$  corresponds to a visit  $x$  months post infection. The number of reads per time point ranges from 7,530 in V33 to 11,806 in V06.

## Results on simulated data

The true sequences and copy numbers are not known for the P018 data. In order to assess the accuracy of our inferred sequence population, we used the HQCSs from a previous FLEA run to simulate a gold standard dataset on which to assess the FLEA pipeline.

The simulation procedure starts with the HQCSs and copy numbers from the FLEA results on P018, then augments them with additional mutated sequences to create a gold standard set of templates. Mutated sequences were added because our clustering strategy may artificially merge similar templates. For each template, noisy reads with a SMRT-style error profile were sampled. Full details of the simulation process appear in the supporting information. These simulated reads were sent through the FLEA pipeline, both with and without frame correction.

The resulting QCS and HQCS sequences were compared to the ground truth using Earth Mover’s Distance (EMD), using normalized copy numbers for the population weights and edit

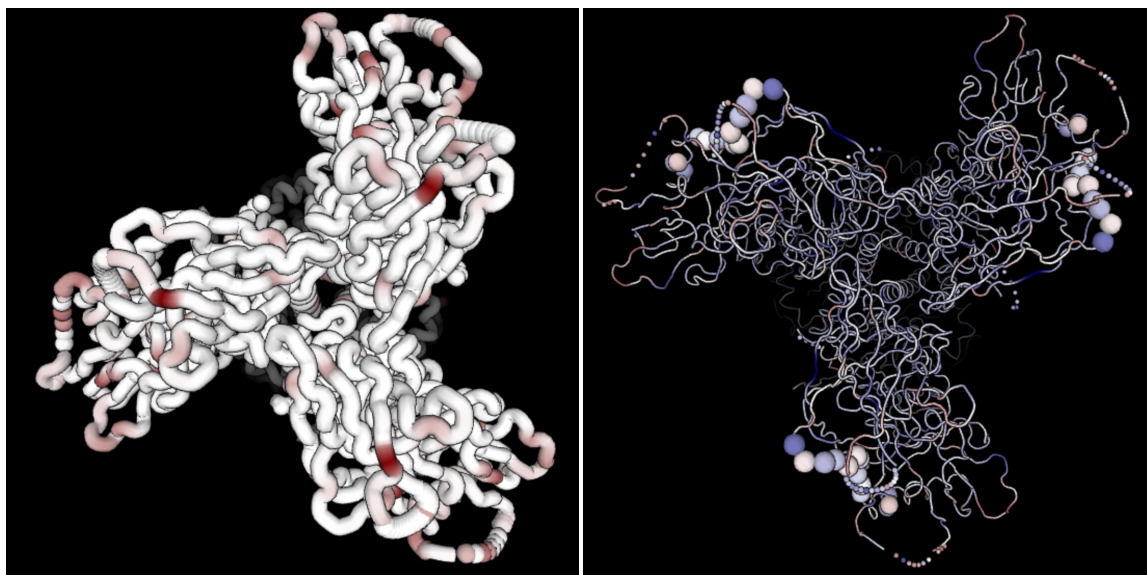


**Figure 7.** Screenshots of the interactive three-dimensional Env structure, colored according to JS divergence (left) and  $dN/dS$  values (right). Positions imputed to be undergoing more positive selection ( $dN/dS > 1$ ) are darker red, and positions undergoing more purifying selection ( $dN/dS < 1$ ) are darker blue. The right structure also shows motif positions highlighted in the sequence viewer.

n	mean errors	consensus type	EMD	$EMD_{FP}$	$EMD_{FN}$
300	9.63	QCS	12.3769	8.3418	2.8956
		HQCS	7.1570	0.4050	5.4271
		HQCS (corrected)	6.4752	0.3020	4.5533
1000	9.63	QCS	10.5433	8.3686	1.2551
		HQCS	2.8279	0.0610	1.1453
		HQCS (corrected)	2.7557	0.0666	1.0405
3000	9.6	QCS	9.5053	8.2837	0.3908
		HQCS	1.6432	0.0146	0.4322
		HQCS (corrected)	1.5168	0.0045	0.2925
10000	9.56	QCS	9.0734	8.3080	0.0782
		HQCS	1.0549	0.0336	0.1735
		HQCS (corrected)	1.0146	0.0073	0.1463

**Table 1.** EMD metrics for various numbers of reads, averaged across all time points. “mean errors” gives the average number of errors in the reads, estimated from the simulated Phred scores.

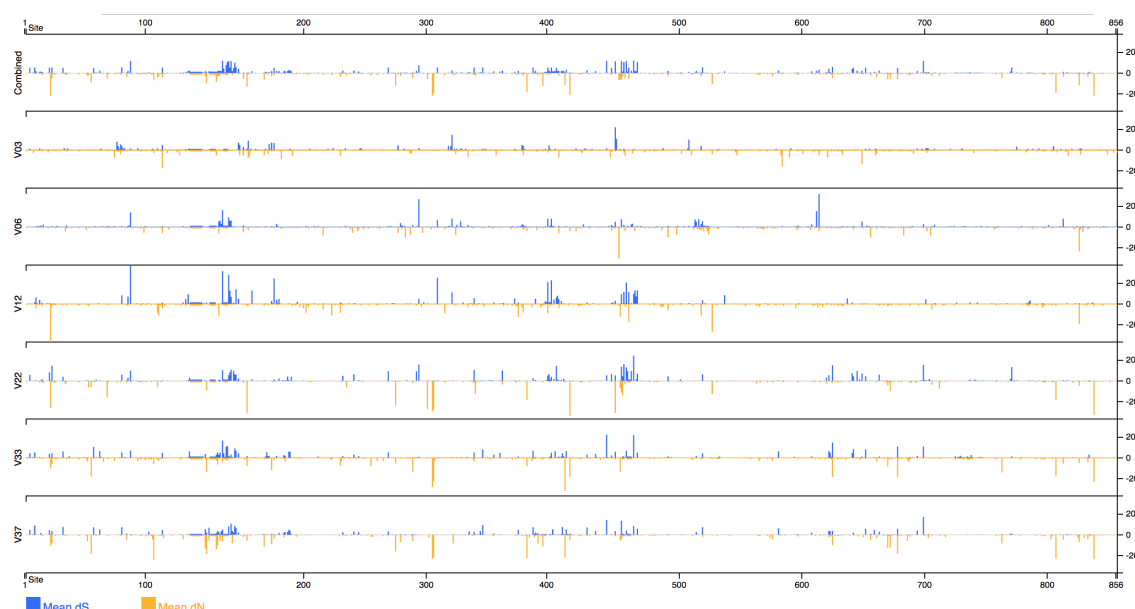


**Figure 8.** Screenshot of dN / dS values mapped to protein positions and separated by time point.

distance for the distance matrix. The fully constrained EMD has units that can be directly interpreted as the average change per nucleotide necessary to transform one sequence population into another. We also calculate two variants of EMD for further insight into how well the inferred population  $B$  estimates the sequences in the ground truth population  $A$ .  $EMD_{FP}$  removes the constraint on  $A$ , allowing any amount of flow from  $A$  to  $B$ . It is a measure of false positives because it grows when  $B$  contains extra sequences distant from any in  $A$ . Similarly,  $EMD_{FN}$  removes the constraint on  $B$ . It grows when  $B$  fails to recapitulate sequences in  $A$ , and therefore is a measure of false negatives.

To see the effect of sequencing runs of different depths, the experiment was repeated for 300, 1,000, 3,000, and 10,000 reads per time point. The results, which appear in Table 1, show the benefit of FLEA's approach of reducing sequence errors via clustering and consensus. The QCS sequences, although they have few false negatives ( $EMD_{FN} = 0.0782$ ) for  $n = 10,000$ , are dominated by false positives ( $EMD_{FP} = 8.3$ ). However, adding the consensus sub-pipeline virtually eliminates false positives ( $EMD_{FP} = 0.0336$ ), at the cost of only a 2.4x increase in false negatives, for a 8.6x improvement in EMD to 1.0549. The frame correction step further improve both  $EMD_{FP}$  and  $EMD_{FN}$  because it turns false positives into true positives.

The full-length *env* sequencing protocol yields approximately 10,000 reads per run; the P018 data averaged 9,744 reads per time point. Therefore, these results with  $n = 10,000$  suggest that FLEA is capable of taking a full sequencing run of CCS reads from a diverse viral population with an average of 9.56 errors per sequence and inferring HQCSs with an average of 1.01 errors per sequence, which corresponds to an average error rate of 0.038%. Moreover, these error rates are mostly caused by low-abundance sequences in both the true population and the inferred FLEA sequences. Figure 10 shows that FLEA perfectly recovers all sequences from all time points that account for at least 1.6% of the population.

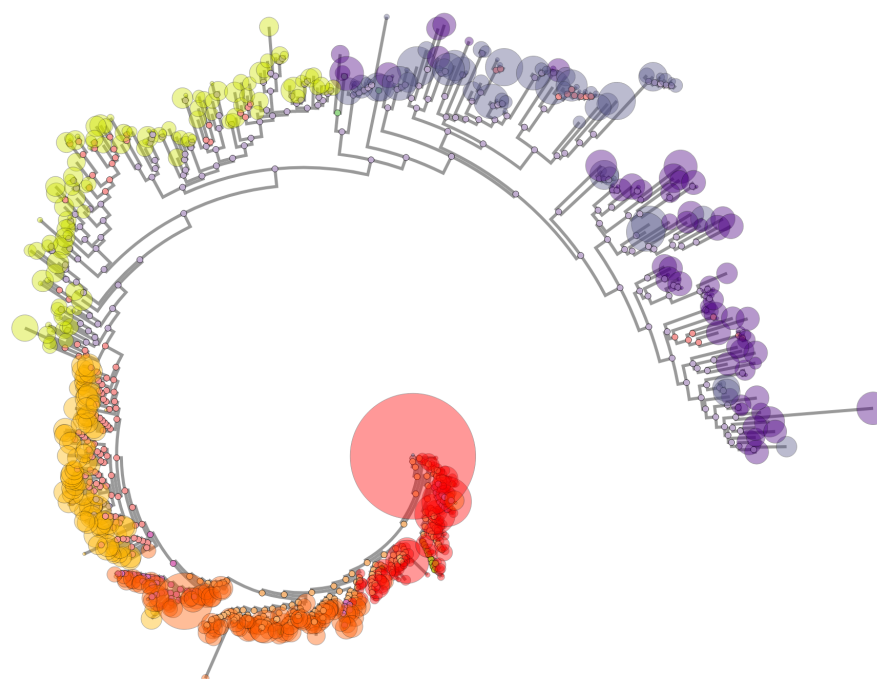


**Figure 9.** Screenshot of the phylogenetic tree viewer. Leaf node size corresponds to sequence copy number. Node color corresponds to time point. Since ancestral sequences have been inferred, ancestral nodes are colored according to the selected motif, which in this case is the N332 glycan supersite.

## Results on real data: donor P018

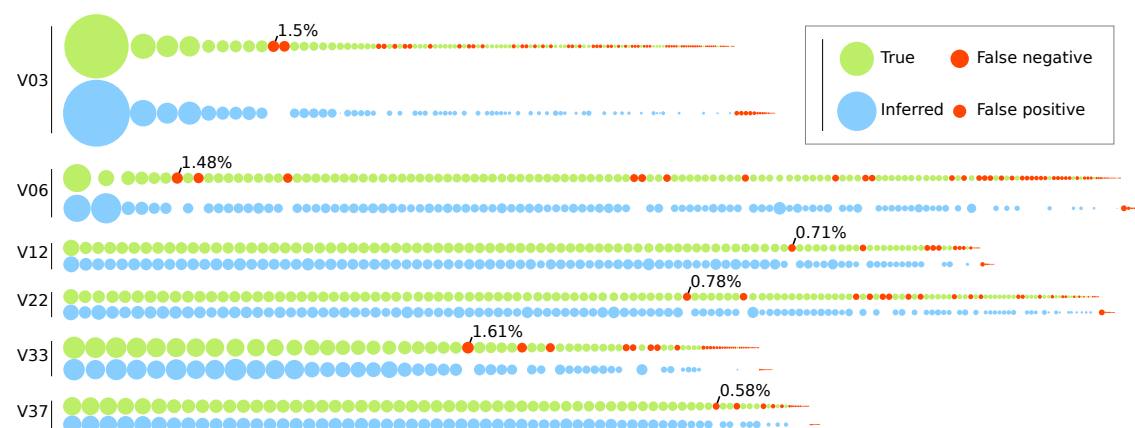
FLEA was run directly on the P018 sequences, and the results are summarized here. The full results of this run are available to view at <http://flea.murrell.group/view/P018>.

Fig. 2 shows the number of sequences from the V03 time point that make it to each stage of the quality and consensus pipelines. At three months post infection, the majority amino-acid sequence variant is shared by 52.1% of the population, and the next most common variants accounts for just 8.66%. This relative lack of diversity is consistent with early infection dynamics. By 37 months post infection there is much more diversity: the most common variant accounts for only 3.96% of the population.

Donor P018 shows signs of potential N332 glycan specificity, as shown by the motif trajectories in Fig. 6. The glycan supersite, centered around N332 in V3, is a common target for broadly-neutralizing antibodies [62] because they are often conserved, so mutations in these regions are associated with escape [63]. A year into sampling (V12), mutations 328R and 330H dominate, and the majority of sequences also contain 339N from 22 months (V22) onwards.

## DISCUSSION

The FLEA pipeline analyzes longitudinal full-length *env* sequences and provides visualizations of the results. Using simulations, we show that FLEA is capable of inferring accurate HIV-1 *env* consensus sequences and population frequencies. Despite each CCS read containing an average of ten errors, our approach distinguishes variants that differ by as little as one base from an amplicon with high indel variation. It uses those high-quality consensus sequences to generate a codon-aware multiple sequence alignment of all time points, estimate ancestral sequences, infer



**Figure 10.** Comparison of true sequence abundances versus copy numbers inferred by FLEA for each time point of the simulated P018 data. Each node represents one sequence, with the area denoting its relative abundance in the population. The true population (top) is colored green. For each true sequence, the matching HQCS sequences appears below it in blue. Red nodes denote false negatives and positives. The most common false negative for each time point is annotated with its abundance.

the phylogenetic tree, and perform many other population-level analyses with high accuracy. These results are presented in a visualization suite that is highly general and applicable to many related sequencing problem.

While our USEARCH-based clustering and consensus strategy for de-noising long PacBio amplicons performs well when error rates are  $< 1\%$ , there is a clear need for more sophisticated long-read de-noising algorithms that exploit the additional depth of lower quality reads that we currently discard. This will be especially beneficial for longer PacBio amplicons, because the CCS read quality distribution degrades with length. For example, while we can currently obtain around 15,000 CCS reads  $< 1\%$  from a P6/C4 RS-II run of our 2.6kb *env* amplicon; this read count drops to  $\sim 1,000$  for full-length 9kb HIV genomes.

Both the pipeline and client-side visualizations are under development, with many improvements planned, including a novel clustering algorithm that reduces false positives and a novel consensus algorithm that uses quality scores and performs frame correction. We plan to integrate epitope prediction into the FLEA pipeline and add appropriate visualizations for the case when users have IC<sub>50</sub> values available for their sequences. Finally, FLEA will be expanded to support other amplicons.

## ACKNOWLEDGMENTS

Research reported here was supported by the National Institute Of Allergy And Infectious Diseases of the National Institutes of Health under Award Numbers R00AI120851 and R01AI120009, and in part by the University of California, San Diego Center for AIDS Research (P30AI036214). K.E. was supported in part by R21AI115701. Computational analysis of sequence data was performed, in part, on a cluster which was supported by U01 GM110749 (NIH/NIGMS). The content is solely the responsibility of the authors and does not necessarily represent the official views of the National Institutes of Health. We are grateful to Sasha Murrell for copy editing.



## REFERENCES

1. DeLeon O, Hodis H, O'Malley Y, Johnson J, Salimi H, Zhai Y, et al. Accurate predictions of population-level changes in sequence and structural properties of HIV-1 Env using a volatility-controlled diffusion model. *PLoS biology*. 2017;15(4).
2. Fischer W, Ganusov VV, Giorgi EE, Hraber PT, Keele BF, Leitner T, et al. Transmission of single HIV-1 genomes and dynamics of early immune escape revealed by ultra-deep sequencing. *PLoS ONE*. 2010;5(8).
3. Henn MR, Boutwell CL, Charlebois P, Lennon NJ, Power KA, Macalalad AR, et al. Whole genome deep sequencing of HIV-1 reveals the impact of early minor variants upon immune recognition during acute infection. *PLoS Pathogens*. 2012;8(3).
4. Leung P, Bull R, Lloyd A, Luciani F. A bioinformatics pipeline for the analyses of viral escape dynamics and host immune responses during an infection. *BioMed research international*. 2014 jan;2014:264519.
5. McCloskey RM, Liang RH, Harrigan PR, Brumme ZL, Poon AFY. An evaluation of phylogenetic methods for reconstructing transmitted HIV variants using longitudinal clonal HIV sequence data. *Journal of virology*. 2014;88(11):6181–94.
6. Pandit A, de Boer RJ. Reliable reconstruction of HIV-1 whole genome haplotypes reveals clonal interference and genetic hitchhiking among immune escape variants. *Retrovirology*. 2014;11:56.
7. Tsibris AMN, Korber B, Arnaout R, Russ C, Lo CC, Leitner T, et al. Quantitative deep sequencing reveals dynamic HIV-1 escape and large population shifts during CCR5 antagonist therapy in vivo. *PLoS ONE*. 2009;4(5):1–12.
8. Highbarger H, Sherman BT, Huang DW, Raley C, Jiang MK, Zheng X, et al. Towards Better Precision Medicine : PacBio Single-Molecule Long Reads Resolve the Interpretation of HIV Drug Resistant Mutation Profiles at Explicit Quasispecies (Haplotype) Level. 2016;(January).
9. Huber M, Metzner KJ, Geissberger FD, Shah C, Leemann C, Klimkait T, et al. MinVar : A rapid and versatile tool for HIV-1 drug resistance genotyping by deep sequencing. *Journal of Virological Methods*. 2017;240:7–13.
10. Lennon N, Berlin AM, Henn MR, Boutwell CL, Charlebois P, Lennon NJ, et al. Whole Genome Deep Sequencing of HIV-1 Reveals the Impact of Early Minor Variants Upon Immune Recognition ... Whole Genome Deep Sequencing of HIV-1 Reveals the Impact of Early Minor Variants Upon Immune Recognition During Acute Infection. 2017;(June).
11. Rithun Mukherjeea, Shane T Jensenb, Frances Malea, Kyle Bittingera RL, Hodinkac, d, Michael D Millere, Bushmana FD. Switching between raltegravir resistance pathways analyzed by deep sequencing. 2012;25(16):1951–1959.
12. Svarovskaia ES, Martin R, McHutchison JG, Miller MD, Mo H. Abundant drug-resistant NS3 mutants detected by deep sequencing in hepatitis C virus-infected patients undergoing NS3 protease inhibitor monotherapy. *Journal of clinical microbiology*. 2012 oct;50(10):3267–74.
13. Gianella S, Delport W, Pacold ME, Young JA, Choi JY, Little SJ, et al. Detection of minority resistance during early HIV-1 infection: natural variation and spurious detection rather than transmission and evolution of multiple viral variants. *J Virol*. 2011 Aug;85(16):8359–67.



14. Backes S, Crumiller M, Bouvier NM, Varble A, Albrecht RA, Backes S, et al. Influenza A Virus Transmission Bottlenecks Are Defined by Infection Route and Recipient Host. 2014;(October).
15. Bull RA, Luciani F, Mcelroy K, Gaudieri S, Pham ST, Cameron B, et al. Sequential Bottlenecks Drive Viral Evolution in Early Acute Hepatitis C Virus Infection. 2011;7(9).
16. Wang GP, Sherrill-Mix Sa, Chang KM, Quince C, Bushman FD. Hepatitis C virus transmission bottlenecks analyzed by deep sequencing. *Journal of virology*. 2010 jun;84(12):6218–28.
17. Gianella S, Pond SLK, Oliveira ME, Scheffler K, Strain MC, De la Torre A, et al. Compartmentalized HIV rebound in the central nervous system after interruption of antiretroviral therapy. *Virus Evolution*. 2016;2(2).
18. Poon AFY, Swenson LC, Bunnik EM, Edo-matas D, Schuitemaker H. Reconstructing the Dynamics of HIV Evolution within Hosts from Serial Deep Sequence Data. 2012;8(11).
19. Kortenhoeven C, Joubert F, Bastos ADS, Abolnik C. Virus genome dynamics under different propagation pressures : reconstruction of whole genome haplotypes of west nile viruses from NGS data. 2015;p. 1–10.
20. Mangul S, Wu NC, Mancuso N, Zelikovsky A, Sun R, Eskin E. Accurate viral population assembly from ultra-deep sequencing data. *Bioinformatics*. 2014;30(12):329–337.
21. Skums P, Mancuso N, Artyomenko A, Tork B, Mandoiu I, Khudyakov Y, et al. Reconstruction of viral population structure from next-generation sequencing data using multicommodity flows. 2013;14(Suppl 9).
22. Wu X, Zhou T, Zhu J, Zhang B, Georgiev I, Wang C, et al. Focused evolution of HIV-1 neutralizing antibodies revealed by structures and deep sequencing. *Science*. 2011;333(6049):1593–602.
23. Yin L, Liu L, Sun Y, Hou W, Lowe AC, Gardner BP, et al. High-resolution deep sequencing reveals biodiversity, population structure, and persistence of HIV-1 quasispecies within host ecosystems. *Retrovirology*. 2012 jan;9:108.
24. Sede MM, Moretti Fa, Laufer NL, Jones LR, Quarleri JF. HIV-1 tropism dynamics and phylogenetic analysis from longitudinal ultra-deep sequencing data of CCR5- and CXCR4-using variants. *PloS one*. 2014 jan;9(7):e102857.
25. Pacold ME, Pond SLK, Wagner GA, Delport W, Bourque DL, Richman DD, et al. Clinical, virologic, and immunologic correlates of HIV-1 intraclade B dual infection among men who have sex with men. *AIDS*. 2012 Jan;26(2):157–65.
26. Capobianchi MR, Giombini E, Rozera G. Next-generation sequencing technology in clinical virology. 2012;.
27. Quinones-mateu ME, Quiñones-mateu ME, Avila S, Reyes-teran G, Martinez MA. Deep Sequencing : Becoming a Critical Tool in Clinical Virology. *Journal of Clinical Virology*. 2015;61(1):9–19.
28. Leung P, Eltahla AA, Lloyd AR, Bull RA, Luciani F. Understanding the complex evolution of rapidly mutating viruses with deep sequencing: beyond the analysis of viral diversity. *Virus research*. 2016;.

29. Vincent AT, Derome N, Charette S. Next-generation sequencing ( NGS ) in the microbiological world : How to make the most of your money. *Journal of Microbiological Methods*. 2016;(March).
30. McElroy K, Thomas T, Luciani F. Deep sequencing of evolving pathogen populations: applications, errors, and bioinformatic solutions. *Microbial informatics and experimentation*. 2014;4(1):1.
31. Beerenwinkel N, Zagordi O. Ultra-deep sequencing for the analysis of viral populations. *Current Opinion in Virology*. 2011;p. 1–6.
32. Rhoads A, Au KF. PacBio Sequencing and Its Applications. *Genomics, Proteomics and Bioinformatics*. 2015;13(5):278–289.
33. Gupta A, Adami C. Strong selection significantly increases epistatic interactions in the long-term evolution of a protein. *PLoS genetics*. 2016;12(3).
34. Parera M, Perez-Alvarez N, Clotet B, Martínez MA. Epistasis among deleterious mutations in the HIV-1 protease. *Journal of molecular biology*. 2009;392(2).
35. Weinreich DM. High-throughput identification of genetic interactions in HIV-1. *Nature genetics*. 2011;43(5).
36. Sarzotti-Kelsoe M, Bailer RT, Turk E, Lin CI, Bilska M, Greene KM, et al. Optimization and validation of the TZM-bl assay for standardized assessments of neutralizing antibodies against HIV-1. *Journal of immunological methods*. 2014;409.
37. Laird Smith M, Murrell B, Eren K, Ignacio C, Landais E, Weaver S, et al. Rapid sequencing of complete env genes from primary HIV-1 samples. *Virus Evolution*. 2016;2(2):vew018.
38. Caskey M, Schoofs T, Gruell H, Settler A, Karagounis T, Kreider EF, et al. Antibody 10-1074 suppresses viremia in HIV-1-infected individuals. *Nature Medicine*. 2017;23(2):185–191. Available from: <http://www.nature.com/doi/10.1038/nm.4268>.
39. Landais E, Murrell B, Briney B, Murrell S, Rantalainen K, Ramos A, et al. Evolutionary features of HIV-1 Env critical for initiation and maturation of broadly neutralizing antibodies to the V2-apex . *Immunity*. 2017;.
40. Liang M, Raley C, Zheng X, Kutty G, Gogineni E, Sherman BT, et al. Distinguishing highly similar gene isoforms with a clustering-based bioinformatics analysis of PacBio single-molecule long reads. *BioData Mining*. 2016;p. 1–13.
41. Di Tommaso P, Chatzou M, Floden EW, Barja PP, Palumbo E, Notredame C. Nextflow enables reproducible computational workflows. *Nature Biotechnology*. 2017;35(4):316–319.
42. Edgar RC. Search and clustering orders of magnitude faster than BLAST. *Bioinformatics*. 2010;26(19):2460–2461.
43. Jacob Schreiber. Pomegranate;. Available from: <https://github.com/jmschrei/pomegranate>.
44. Foley BT, Leitner TK, Apetrei C, Hahn B, Mizrahi I, Mullins J, et al. HIV Sequence Compendium 2017. Los Alamos National Lab.(LANL), Los Alamos, NM (United States); 2017.

45. Edgar RC, Flyvbjerg H. Error filtering, pair assembly and error correction for next-generation sequencing reads. *Bioinformatics*. 2015;31(21).
46. Katoh K, Misawa K, Kuma Ki, Miyata T. MAFFT: a novel method for rapid multiple sequence alignment based on fast Fourier transform. *Nucleic acids research*. 2002;30(14):3059–3066.
47. Pond SLK, Muse SV. HyPhy: hypothesis testing using phylogenies. In: *Statistical methods in molecular evolution*. Springer; 2005. p. 125–181.
48. Ratner L, Haseltine W, Patarca R, Livak KJ, Starcich B, Josephs SF, et al. Complete nucleotide sequence of the AIDS virus, HTLV-III. *Nature*. 1985;313(6000):277–284.
49. Price MN, Dehal PS, Arkin AP. FastTree: computing large minimum evolution trees with profiles instead of a distance matrix. *Molecular biology and evolution*. 2009;26(7):1641–1650.
50. Price MN, Dehal PS, Arkin AP, et al. FastTree 2—approximately maximum-likelihood trees for large alignments. *PloS one*. 2010;5(3):e9490.
51. Hasegawa M, Kishino H, Yano Ta. Dating of the human-ape splitting by a molecular clock of mitochondrial DNA. *Journal of molecular evolution*. 1985;22(2).
52. Sergei L Kosakovsky Pond. TN93;. Available from: <https://github.com/veg/tn93>.
53. Tamura K, Nei M. Estimation of the number of nucleotide substitutions in the control region of mitochondrial DNA in humans and chimpanzees. *Molecular biology and evolution*. 1993;10(3).
54. Torgerson WS. Multidimensional scaling: I. Theory and method. *Psychometrika*. 1952;17(4).
55. David Cournapeau. scikit-learn;. Available from: <https://scikit-learn.org>.
56. Murrell B, Moola S, Mabona A, Weighill T, Sheward D, Pond SLK, et al. FUBAR: a fast, unconstrained bayesian approximation for inferring selection. *Molecular biology and evolution*. 2013;p. mst030.
57. Ember Core Team. Ember.js;. Available from: <https://emberjs.com/>.
58. Mike Bostock, Jason Davies, Jeffrey Heer, Vadim Ogievetsky, and community. D3.js;. Available from: <http://d3js.org/>.
59. Lee JH, Ozorowski G, Ward AB. Cryo-EM structure of a native, fully glycosylated, cleaved HIV-1 envelope trimer. *Science*. 2016;351(6277):1043–1048.
60. Marco Biasini. pv;. Available from: <http://biasmv.github.io/pv/>.
61. Sergei L Kosakovsky Pond. phylotree.js;. Available from: <https://github.com/veg/phylotree.js>.
62. Landais E, Huang X, Havenar-Daughton C, Murrell B, Price MA, Wickramasinghe L, et al. Broadly Neutralizing Antibody Responses in a Large Longitudinal Sub-Saharan HIV Primary Infection Cohort. *PLoS Pathogens*. 2016;12(1):1–22.
63. Deshpande S, Patil S, Kumar R, Hermanus T, Murugavel KG, Srikrishnan AK, et al. HIV-1 clade C escapes broadly neutralizing autologous antibodies with N332 glycan specificity by distinct mechanisms. *Retrovirology*. 2016;13(1):60.